RESEARCH ARTICLE

Key Point:
- Cloud-controlled sunlight in June drives Arctic sea ice loss in August–October

Correspondence to:
Y.-S. Choi,
ysc@ewha.ac.kr

Connecting early summer cloud-controlled sunlight and late summer sea ice in the Arctic

Yong-Sang Choi[1], Baek-Min Kim[2], Sun-Kyong Hur[3], Seong-Joong Kim[2], Joo-Hong Kim[2], and Chang-Hoi Ho[3]

[1]Department of Environmental Science and Engineering, Ewha Womans University, Seoul, South Korea, [2]Korea Polar Research Institute, Incheon, South Korea, [3]School of Earth and Environmental Sciences, Seoul National University, Seoul, South Korea

Abstract This study demonstrates that absorbed solar radiation (ASR) at the top of the atmosphere in early summer (May–July) plays a precursory role in determining the Arctic sea ice concentration (SIC) in late summer (August–October). The monthly ASR anomalies are obtained over the Arctic Ocean (65°N–90°N) from the Clouds and the Earth's Radiant Energy System during 2000–2013. The ASR changes primarily with cloud variation. We found that the ASR anomaly in early summer is significantly correlated with the SIC anomaly in late summer (correlation coefficient, $r \approx -0.8$ with a lag of 1 to 4 months). The region exhibiting high (low) ASR anomalies and low (high) SIC anomalies varies yearly. The possible reason is that the solar heat input to ice is most effectively affected by the cloud shielding effect under the maximum TOA solar radiation in June and amplified by the ice-albedo feedback. This intimate delayed ASR-SIC relationship is not represented in most of current climate models. Rather, the models tend to over-emphasize internal sea ice processes in summer.

1. Introduction

Arctic sea ice has undergone rapid retreat over recent decades [e.g., *Comiso et al.*, 2008; *Stroeve et al.*, 2008], and its summer extent reached the lowest level in 2012 according to the records of the past 1450 years [*Kinnard et al.*, 2011]. It has been suggested that the accelerated Arctic sea ice loss may have been the consequence of the rapid reduction in Arctic multi-year sea ice by the ice movement and atmospheric thermodynamic processes [*Francis et al.*, 2005; *Lindsay and Zhang*, 2005]. Although an increasing number of studies attribute the recent sea ice loss to global warming forcing [*Min et al.*, 2008; *Kay et al.*, 2011], the forced sea ice changes have not been quantitatively distinguished [*Polyakov et al.*, 2010; *Day et al.*, 2012].

There have been numerous studies investigating the controlling factors for the Arctic sea ice concentration (SIC). First, thermodynamic processes take place through energy exchanges between the ocean, sea ice, and the atmosphere, changing SIC through the surface and bottom heat fluxes of sea ice [*Kapsch et al.*, 2013; *Stroeve et al.*, 2014; and references therein]. Second, dynamic processes can promote the changes in SIC by transport to warmer regions via atmospheric winds and ocean currents [*Kwok*, 2009; *Stroeve et al.*, 2014]. A dynamic process to fracture sea ice floes by strong surface winds and waves can also be effective [*Parkinson and Comiso,* 2013]. These thermodynamic and dynamic processes are in fact highly coupled, as the surface wind can bring warm moist air and induce ocean warming via vertical mixing [*Zhang et al.*, 2013]. A number of studies attempted to relate atmospheric sources of variability with sea ice reduction. In particular, it has been suggested that positive phases of the leading mode of winter Northern hemispheric sea level pressure variability, the Arctic oscillation (AO) drove the sea ice decrease in the 1990s (e.g., *Rigor et al.* [2002]; *Zhang et al.* [2003]; *Kwok et al.* [2004]) and the transformation of the AO pattern accelerated sea ice decrease after the 1990s (e.g., *Zhang et al.* [2008]; *Overland and Wang* [2010]).

Although the aforementioned physical processes that control the SIC have been extensively studied, seasonal to longer-term prediction of SIC using the state-of-the-art climate models is still not promising [*Stroeve et al.*, 2012a]. This is perhaps because our understanding of processes regarding the sea ice melt is still lacking. In particular, the role of cloud variation and its control of absorbed solar radiation (ASR) have not been sufficiently investigated mainly due to the lack of reliable cloud observations in the Arctic [*Ackerman*

Table 1. The Correlation Coefficients Between Absorbed Solar Radiation (ASR) and the Cloud and Surface Parameters Area Averaged Over the Arctic Ocean (65°N–90°N)

Month	α_{tot}	$(1-f)\,\alpha_s$	$f\,\alpha_c$	α_s	α_c	f
	Correlation Coefficient (Covariance)					
April	−0.95[a] (−0.02)	−0.51[b] (−0.04)	0.23 (0.02)	−0.66[a] (−0.01)	−0.78[a] (−0.02)	0.45 (4.83)
May	−0.98[a] (−0.02)	−0.49[b] (−0.03)	−0.08 (0.01)	−0.49[b] (−0.02)	−0.77[a] (−0.02)	0.39 (3.16)
June	−1.00[a] (−0.08)	0.24 (0.03)	−0.86[a] (−0.12)	−0.93[a] (−0.09)	−0.78[a] (−0.08)	−0.55[b] (−10.59)
July	−0.99[a] (−0.06)	0.48[b] (0.02)	−0.95[a] (−0.08)	−0.73[a] (−0.05)	−0.94[a] (−0.04)	−0.86[a] (−9.50)
August	−0.97[a] (−0.04)	−0.25 (−0.003)	−0.92[a] (−0.04)	−0.80[a] (−0.06)	−0.91[a] (−0.03)	−0.61[b] (−2.98)
September	−0.90[a] (−0.02)	−0.43 (−0.01)	−0.81[a] (−0.02)	−0.85[a] (−0.03)	−0.85[a] (−0.02)	−0.16 (−0.43)
October	−0.79[a] (−0.01)	−0.57[b] (−0.01)	−0.67[a] (−0.003)	−0.76[a] (−0.01)	−0.71[a] (−0.01)	0.27 (0.31)

[a]Regressions validated to the 99% confidence level.
[b]Regressions validated to the 95% confidence level.
Values in parentheses are the corresponding covariances.

et al., 2008]. ASR plays an important role in the process of sea ice melting over the summer, since ASR is a major energy source in the Arctic Ocean [*Perovich et al.*, 2008, 2011; *Stroeve et al.*, 2012b, 2014]. A large portion of the incoming solar radiation penetrating the clouds (or the atmosphere if no clouds are present) was known to not only melt the ice surface but also lead to the basal and lateral melting owing to the warming of the upper ocean [*Perovich et al.*, 2008]. This melting process may have led to the increase in the length of melting season [*Stroeve et al.*, 2014], increasing the cumulative total ASR by the ice/ocean system. Therefore, the observed increase in ASR was suggested as an important factor for the long-term decline of Arctic sea ice observed over the last few decades [*Lindsay and Zhang*, 2005; *Stroeve et al.*, 2014] and also for the record-breaking retreat of Arctic sea ice in a particular year (e.g., 2007 and 2012) [*Kay et al.*, 2008; *Perovich et al.*, 2008; *Zhang et al.*, 2008].

For the summer of 2007, it has been suggested that the low Arctic sea ice extent begins with a decrease in cloud cover (and, therefore, an increase in ASR) during early summer [*Kay et al.*, 2008; *Kay and L'Ecuyer*, 2013]. However, the contribution of Arctic cloud to sea ice melt through the control of ASR has not yet been clearly evaluated [*Kay and Gettelman*, 2009; *Schweiger et al.*, 2008]. Moreover, there remains a question as to whether cloud variations actually lead ice melt in the summer or not [*Francis et al.*, 2005; *Kapsch et al.*, 2013]. This study attempts to clarify the relationship between cloud, ASR, and SIC with due consideration of the timescales of sea ice melting processes using satellite observations described in the next section.

2. Data and Methods

Monthly gridded sea ice data were collected over the Arctic region (65°N–90°N) from the Hadley Centre sea ice and sea surface temperature dataset (HadISST1) [*Rayner et al.*, 2003]. The data are available from 1870 to present, with a resolution of 1°×1°. Here, the SIC value is the percentile (from 15 to 100%) of the sea ice fraction (from 0.15 to 1).

Monthly gridded radiative fluxes and cloud data were obtained from the Clouds and the Earth's Radiant Energy System (CERES) [*Wielicki et al.*, 1996]. CERES is the only space-borne radiometer directly measuring global, top-of-atmosphere (TOA) outgoing broadband shortwave fluxes (0.3 to 5 μm). The TOA parameters are available for the period from March 2000 to September 2013 in the CERES ES4 Terra Xtrk Edition 3 product with a resolution of 2.5°×2.5°. Cloud properties (e.g., cloud fraction, cloud optical depth, and cloud top pressure) were also obtained for the same 13 year period from the CERES SYN1deg (Synoptic Radiative Fluxes and Clouds) Edition 3A product. The SYN1deg data were derived from the CERES cloud algorithm using the Moderate Resolution Imaging Spectro-radiometer and 3-hourly geostationary satellite cloud properties. In this paper, for the purpose of comparison between SIC and satellite data, the former data set was degraded to a resolution of 2.5°×2.5°.

CERES measures solar energy fluxes at TOA directly (in ES4) with the uncertainty of approximately 5% [*CERES Science Team*, 2013], and derived retrievals of surface solar energy fluxes (in SYN1deg) would have additional uncertainties [*Kato et al.*, 2012]. Therefore, we focus on TOA rather than the surface estimates, although both ASR at the TOA and at the surface are shown in this study. ASR obtained in this study is therefore expected to be proportional to both the total-sky co-albedo ($1 - \alpha_{tot}$) and the incident solar radiation at
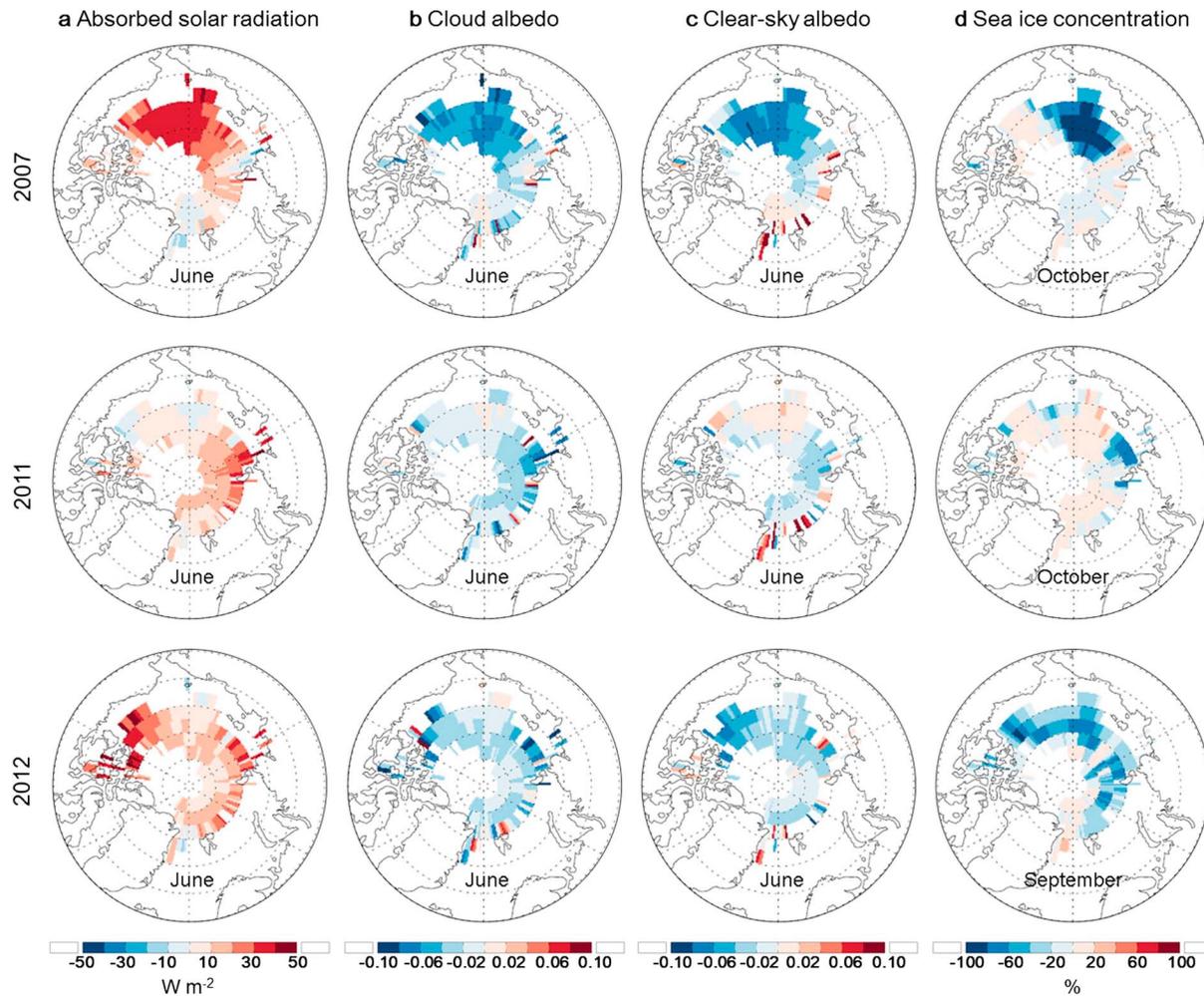
Figure 1. Regional distribution of the anomalies of (a) absorbed solar radiation (ASR), (b) the cloud albedo, and (c) the clear-sky albedo, all for June 2007, 2011, and 2012, and (d) sea ice concentration (SIC) for October 2007 and 2011 and September 2012. In these years, record-breaking minimal SIC was observed. Note that these figures do not include the regions where total SIC for August, September, and October were less than 15% or the regions with permanent SIC throughout the year.

TOA (S_0). α_{tot} is the ratio of the reflected radiation flux to S_0 for the total-sky area. Since α_{tot} and S_0 are available in the CERES ES4 data, ASR can be calculated for each 2.5° grid for the Arctic Ocean using equation (1):

$$\text{ASR} = (1-\alpha_{tot})S_0. \qquad (1)$$

Of the entire domain, the area with missing solar radiation data accounts for 78% in January, 33% in February, 11% in October, 67% in November, 100% in December, and 0% for the remaining months. Thus, calculation of ASR was limited for the December period owing to the lack of solar radiation. The α_{tot} can be further broken down into the clear-sky and cloudy-sky reflections, both of which contribute to ASR variations. Atmospheric absorption and scattering effects of solar radiation are secondary in contributing to ASR variations. In addition, there is a radiation component that partly penetrates clouds and reflects from the surface. However, this is also negligible in contributing to ASR variations, unless cloud opacity is very low. As we will show later, the ASR anomaly from TOA fluxes in ES4 data—equation (1)—is almost identical to the ASR anomaly from the surface fluxes in SYN1deg data. This supports that contribution of the atmosphere to ASR variations is minor. Therefore, the reflection of solar radiation actually arises from clear-sky albedo (α_s) and cloud albedo (α_c), as described by equation (2):

$$\alpha_{tot} = (1-f)\alpha_s + f\alpha_c. \qquad (2)$$

This single-layer cloud model, or its equivalent, has been widely used in studies of radiative transfer and satellite retrievals in partly cloudy environment with cloud fraction f [*Ramanathan*, 1987; *Coakley et al.*, 2005].
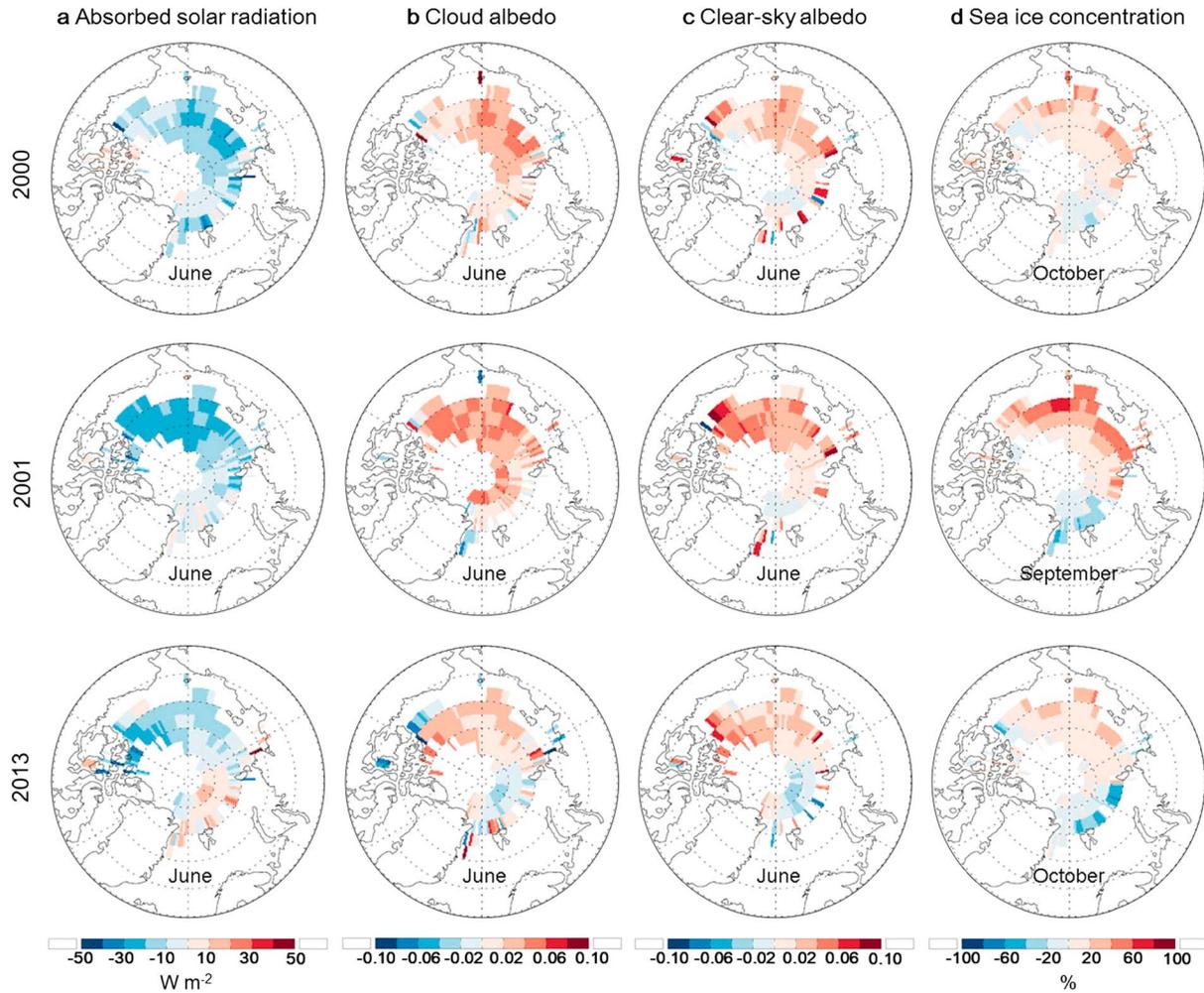
Figure 2. The same as Figure 1, but for 2000, 2001, and 2013. The corresponding months are marked. In October 2000 and September 2001, record-breaking maximal SIC was observed. The year 2013 was additionally shown since it was rarely reported in the other literatures.
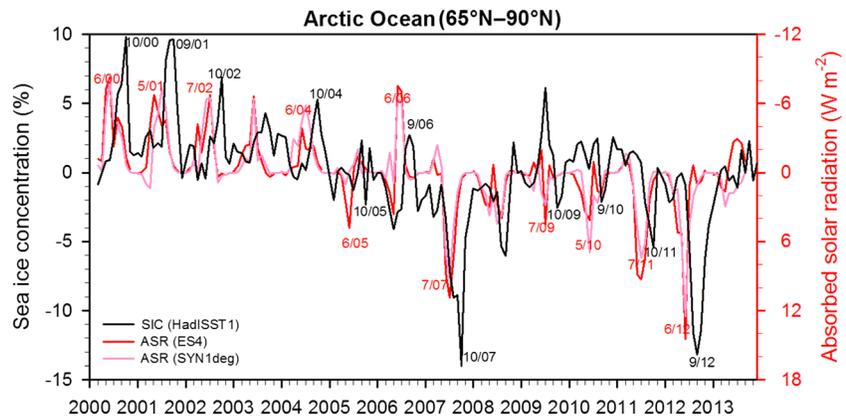

Figure 3. Time series of monthly anomalies of SIC (%, in black), ES4 ASR (W m^{-2}, in red), and SYN1deg ASR (W m^{-2}, in pink) area averaged over the Arctic Ocean (65°N–90°N) from March 2000 to December 2013. Note that the axis of the ordinate for ASR (the right axis) is reversed for better comparison. The months and years in which distinctively high or low values were found are noted.
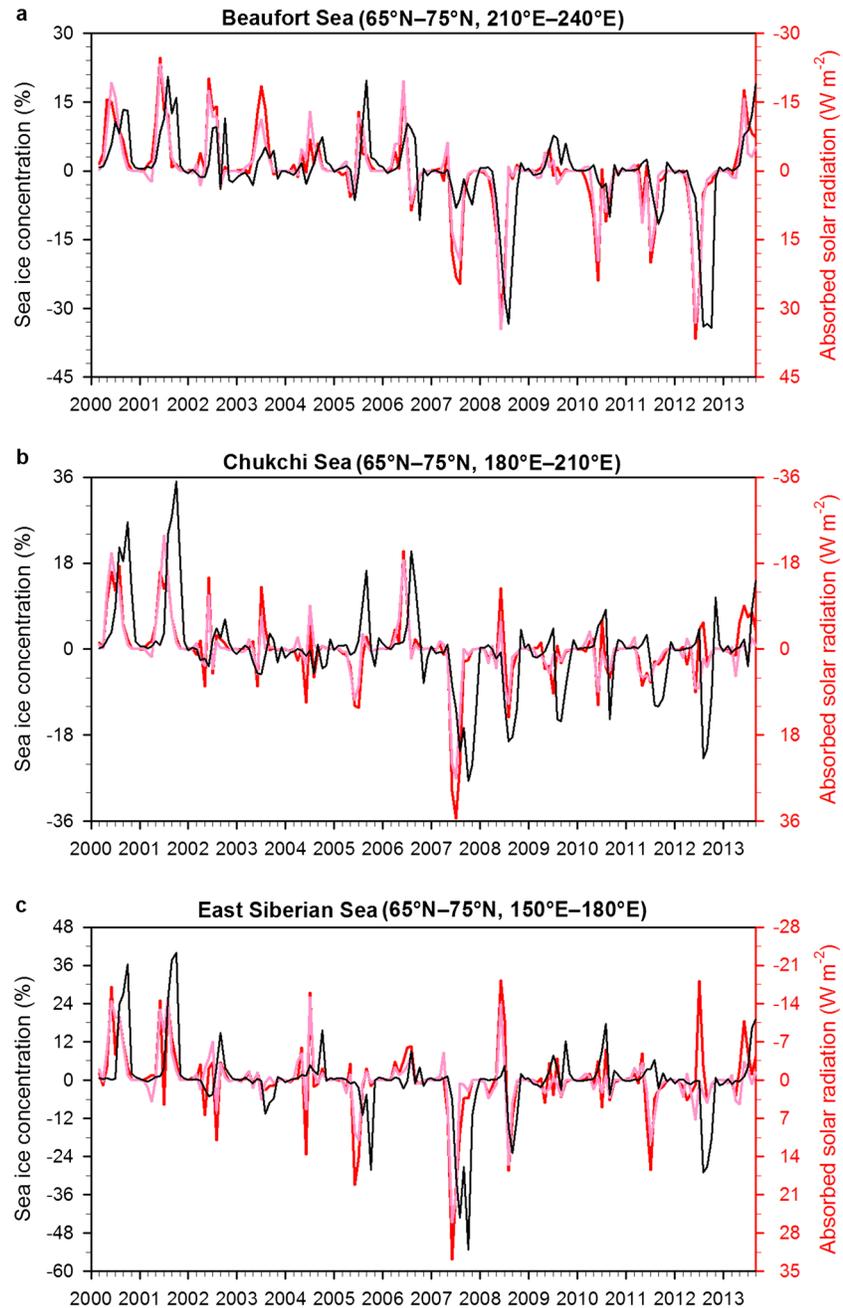
Figure 4. The same as Figure 3, but for three regions, Beaufort Sea (65°N–75°N, 210°E–240°E), Chukchi Sea (65°N–75°N, 180°E–210°E), and East Siberian Sea (65°N–75°N, 150°E–180°E).

The parameters α_{tot}, f, and α_s are available in the CERES ES4 data. α_s is determined by ratioing upward solar radiation to S_0 for clear-sky scene [*Chang et al.*, 2013]. f in the CERES ES4 data is obtained originally from the passive sensor, MODIS, and therefore f in the Arctic could be less reliable than the other regions [*Ackerman et al.*, 2008]. However, *Kay and L'Ecuyer* [2013] showed that the Arctic cloud changes obtained by an active sensor, CALIOP, are comparable to cloud changes from MODIS over the same period. Thus, α_c is the only value that was derived from the formula with other available parameters $(\alpha_{tot} - (1 - f)\,\alpha_s)\,/\,f$.

The area average of ASR over the Arctic Ocean ([ASR]) was considered at first. In order to remove the influence of a strong seasonal cycle of [ASR], the ASR anomaly for each month was estimated by subtracting the climatological means (over the whole period of data) of [ASR] for the corresponding month from the original
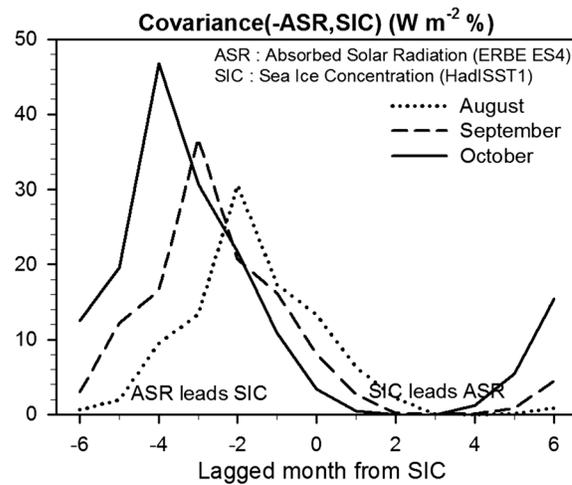
Figure 5. Lagged covariances of $-$ASR and SIC (W m^{-2} %). $-$ASR denotes $-1 \times$ ASR. The results for SICs only in August, September, and October are shown.

monthly [ASR] value. The same process was applied to obtain the SIC anomaly. Hereafter, SIC and ASR denote the monthly anomalies.

The Coupled Model Intercomparison Project Phase 5 (CMIP5) climate models [*Taylor et al.*, 2011] have also been used to evaluate the capability in reproducing the observed cloud-ASR-SIC relationship. Based upon historical runs of 38 available models, a 40 year period (1961–2000) of TOA downwelling/upwelling shortwave fluxes and SIC data was selected. Only the first ensemble member (i.e., *r1i1p1*) of each model's historical run is considered here. The modeled ASR was obtained by subtracting the upwelling shortwave flux from the downwelling shortwave flux. The overall conclusions based on the CMIP5 models were insensitive to the length of the selected period.

3. Relationship Between Early Summer ASR and Late Summer SIC

3.1. Observational Features

Table 1 shows the correlation coefficients (r) and covariances between ASR and the terms in equations (1) and (2). ASR is negatively correlated with the cloud reflection (i.e., $f\,\alpha_c$), for June to October ($r = -0.95$ to -0.67); the r values are significant at the 99% confidence level. Covariance of ASR and $f\,\alpha_c$ is the greatest in June. However, the correlation between ASR and clear-sky reflection ($(1 - f)\,\alpha_s$) was found to be positive for June and July though it is statistically insignificant at the 99% confidence level. The positive correlation may be due to the influence of sea ice melt that may increase evaporation from the open sea. The resultant moisture supply would increase f and decrease ASR [*Kapsch et al.*, 2013]. Thus, the correlation between f and ASR is negative, but the correlation between $(1 - f)\,\alpha_s$ and ASR is positive over sea ice retreat area in June and July. Unlike $(1 - f)\,\alpha_s$, the clear-sky albedo (α_s) alone is consistently negatively correlated with ASR for all months (significant at the 95% confidence level), as similarly noted by *Riihelä et al.* [2013]. The cloud albedo (α_c) should be also negatively correlated with ASR since low cloud albedo essentially leads to more ASR.

Exceptionally, we found that in April, May, and October, correlations between f and ASR are positive. The positive correlations result from a high solar zenith angle. The solar radiation reflected from a surface depends on the solar zenith angle. The surface albedo under clear skies increases dramatically as the solar zenith angle increases (i.e., the sun approaches the horizon), whereas under a sufficiently thick cloud the surface albedo is insensitive to the location of the sun. Thus, cloudiness decreases the surface albedo when the solar zenith angle is high ($>$ ~55°) [*Hartmann*, 1994]. This corresponds to the high latitudes of the Arctic in April, May, and October. In the other months, the solar zenith angle becomes low, and the positive ASR-f correlation disappears. Therefore, the monthly variations in ASR in the Arctic region can be explained by cloud reflection (i.e., $f\,\alpha_c$) for most summer months (June to October), but by clear-sky reflection (i.e., $(1 - f)\,\alpha_s$) for the rest of the period (April, May, and October). Thus, the contribution of f to the variation of ASR is dependent on the period.

To closely examine the cloud-ASR relationship, ASR, cloud albedo, and clear-sky albedo were compared for 2007, 2011, and 2012 (when the record-breaking low SICs were observed) (Figure 1). We show SIC for October 2007 and 2011 and September 2012 because the minimal SICs were observed in these months. Note that, the choice of the month does not affect the conclusion. It is important to note that the region exhibiting high ASR anomalies is not stationary but rather varies yearly. A clear spatial correlation was found among anomalously high ASR, low cloud albedo (or cloud optical depth), low clear-sky albedo, and low SIC. The low SIC anomalies in September or October are mainly distributed in the latitudinal band between 75°N and 85°N, which corresponds to the transition zone between first-year ice and multi-year ice in recent years.
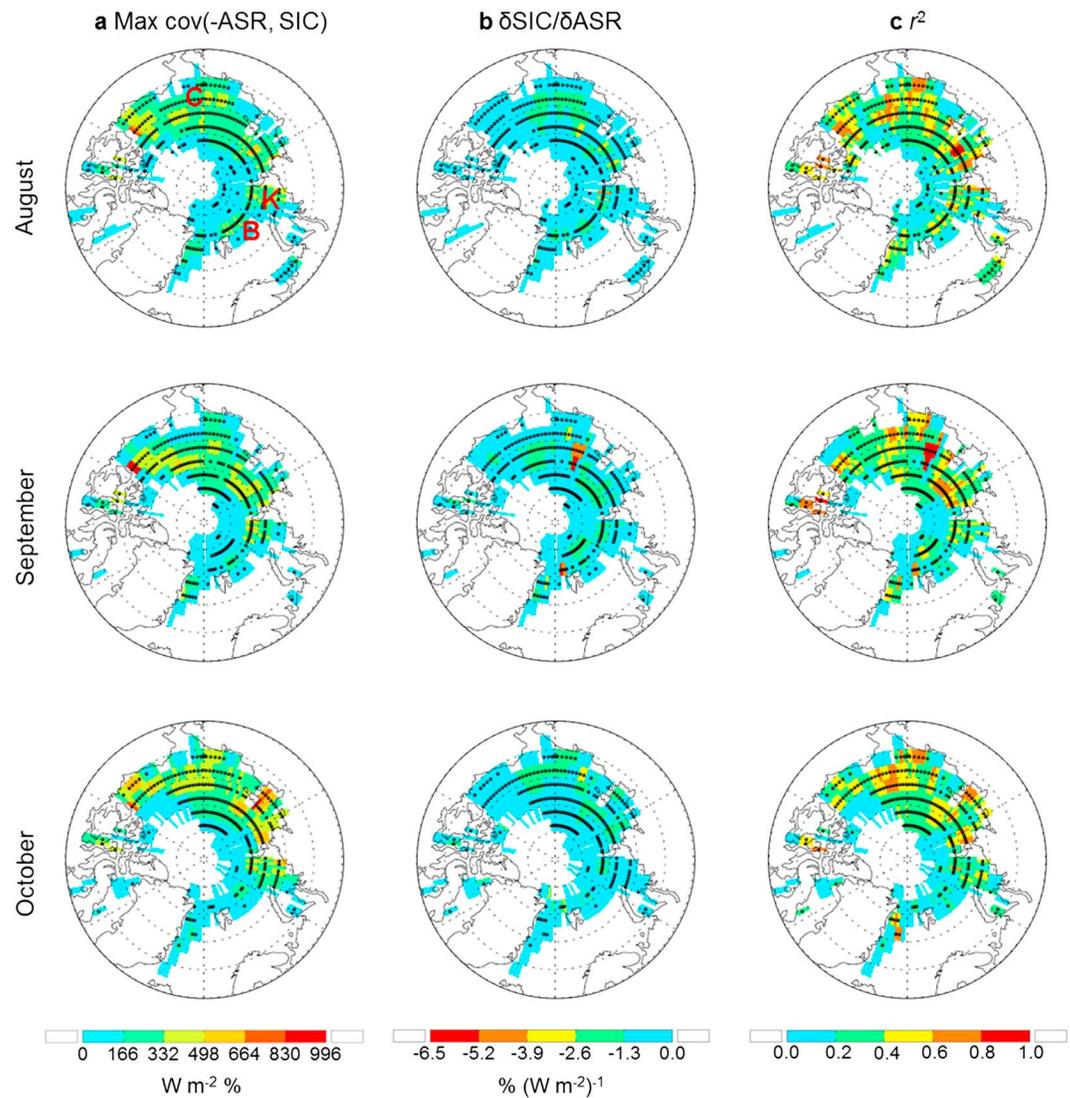
Figure 6. Spatial distributions of the relation between ASR in early summer and SIC in late summer, (a) the maximal covariance of −ASR and SIC, (b) δSIC/δASR, and (c) the coefficient of determination for the regression of SIC on ASR. Both Figures 6b and 6c correspond to Figure 6a. The figures describe data for (top) August, (middle) September, and (bottom) October sea ice. The black dots indicate statistical significance at the 95% confidence level.

The spatial pattern of low SIC anomalies in September or October for each year is moderately comparable with that of clear-sky albedo anomalies in June, meaning that SIC in late summer might be also related to the initial state of sea ice albedo that is presented by clear-sky albedo in June. In addition, the present study did not find significant correlations between ASR anomalies and other cloud parameters such as cloud top pressure, and low-level atmospheric horizontal winds (figures not shown). These results suggest that, in recent years of minimal summer SIC, there have been high anomalies of ASR and low anomalies of cloud albedo in early summer in the Arctic region.

On the contrary, the years 2000 and 2001 with maximal SIC in the late summer months show low anomalies of ASR and high anomalies of cloud albedo in the Arctic region (Figure 2). This is also true for the latest year 2013 with slightly positive SIC anomaly in October. These indicate the importance of Arctic clouds for the late summer SIC anomaly, in either cases of minimal and maximal SICs.

We expanded the analysis for the whole available years from 2000 to 2013. Figure 3 compares the time series of ES4 ASR (red), SYN1deg ASR (pink), and SIC (black) anomalies over the entire Arctic region. Both of the SIC minima in recent years (particularly in October 2007 and 2011, and in September 2012)

Table 2. Areal Fraction of Sea Ice for a Range of r^2 of Sea Ice Concentration (SIC) on ASR, and the Corresponding Mean δSIC/δASR[a]

Sea Ice Type	Month	r^2	0.0–0.2	0.2–0.4	0.4–0.6	0.6–0.8	0.8–1.0
First-year ice	August SIC	Area (%)	34.5	43.7	15.2	6.6	0.0
		δSIC/δASR (% (W m^{-2})$^{-1}$)	−0.2	−0.6	−1.0	−1.4	—
	September SIC	Area (%)	38.8	33.7	19.2	8.4	0.0
		δSIC/δASR (% (W m^{-2})$^{-1}$)	−0.2	−0.6	−0.8	−1.2	—
	October SIC	Area (%)	45.4	27.7	15.9	10.9	0.0
		δSIC/δASR (% (W m^{-2})$^{-1}$)	−0.5	−0.9	−1.5	−1.7	—
Multi-year ice	August SIC	Area (%)	31.9	35.7	23.4	7.9	1.1
		δSIC/δASR (% (W m^{-2})$^{-1}$)	−0.3	−0.8	−1.4	−1.7	−2.0
	September SIC	Area (%)	32.9	40.5	16.4	6.9	3.5
		δSIC/δASR (% (W m^{-2})$^{-1}$)	−0.5	−1.1	−1.3	−2.4	−3.9
	October SIC	Area (%)	38.6	36.6	19.1	5.7	0.0
		δSIC/δASR (% (W m^{-2})$^{-1}$)	−0.3	−1.0	−1.3	−1.8	—
Total	August SIC	Area (%)	32.8	38.5	20.6	7.4	0.7
		δSIC/δASR (% (W m^{-2})$^{-1}$)	−0.3	−0.8	−1.3	−1.6	−2.0
	September SIC	Area (%)	34.5	38.6	17.1	7.3	2.5
		δSIC/δASR (% (W m^{-2})$^{-1}$)	−0.4	−1.0	−1.2	−2.0	−3.9
	October SIC	Area (%)	41.3	33.1	17.9	7.7	0.0
		δSIC/δASR (% (W m^{-2})$^{-1}$)	−0.4	−0.9	−1.3	−1.7	—

[a]Perennial sea ice is excluded in the total sea ice area.

and the SIC maxima in October 2000 and September 2001 are clearly shown. Besides these particular extreme cases, 4 month leads of ASR with respect to SIC are consistently observed through the entire period in Figure 3. Note that even in the early 2000s, every SIC maxima followed ASR minima. Therefore, there is a clear negative lag correlation between ASR and SIC anomalies. The SIC anomaly in recent years can be mainly attributed to multi-year ice, as shown in Figures 1 and 2. Thus, SIC in late summer could be sensitive to the ASR anomaly in June.

In addition, the lagged correlation remains apparent for major sea ice loss regions (at 2 month lag, minimum lagged $r = −0.75$ for the Beaufort Sea, $−0.57$ for the Chukchi Sea, and $−0.42$ for the East Siberian Sea) (Figure 4). There are few opposed cases of low anomalies of both the early summer ASR and the late summer SIC occur in the East Siberian Seas in the years 2008 and 2012. For June 2012, moreover, the TOA ASR (ES4 ASR in red) is exceptionally low, while the surface ASR (SYN1deg ASR in pink) is high and consistent with the following low SIC. This difference between the TOA and surface ASRs could be due to atmospheric scattering, which plays a role in some local areas.

It might be argued that the lagged correlation between ASR and SIC shown in Figures 3 and 4 may be a natural consequence of seasonal cycles. Incoming solar energy is greatest in June (when there are a full 24 h of daylight around the summer solstice) in comparison to other months of the year. However, this research refers to ASR as "the monthly anomaly" of area-averaged and deseasonalized data over the Arctic region. The deseasonalized data do not necessarily mean that largest variance of the June ASR is reduced. Rather, ASRs in June often have either the maxima or minima because of largest variance of the raw ASR data in June. Namely, ASRs in June are not always the maxima throughout the year, but rather the minima for many years. Similarly, SICs in Octobers are not always the minima throughout the year. As a result, ASR in June and SIC in October are not necessarily anti-correlated simply owing to seasonal cycles. In addition, it appears that spring SIC is not related to late summer SICs, and thus it is not an initial low SIC that leads to late summer SICs.

To quantitatively represent the ASR-SIC relationship, the covariance of −ASR (indicating $−1 \times$ ASR) and SIC in August, September, and October were calculated separately (as shown in Figure 5). The greatest covariance for ASR was observed for June, while the greatest covariance for SIC was observed in the late summer months of August, September, and October. This implies that Arctic SIC in the late summer months may largely be determined by ASR of June. Figure 5 also displays that there is nearly zero covariance of ASR and SIC at both zero and positive lags, indicating that, when ASR is absent during the winter months, it cannot respond to the late summer SIC regardless of the month. This has important implications for sea ice shortwave radiation feedback in the Arctic. For example, Arctic sea ice in the late summer was less likely to be leading but more likely to be responding to ASR, which is primarily controlled by cloud reflection ($f \alpha_c$) (Table 1).
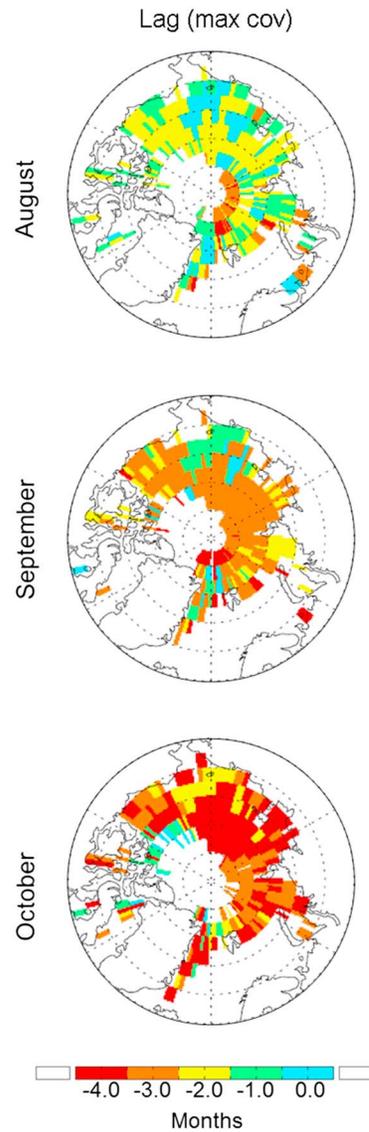
Figure 7. Spatial distributions of the maximal covariance lag and first/multi-year sea ice. The maximal covariance lag of ASR and SIC is from −4 to 0 month; the negative lag means ASR is ahead of SIC.

This result agrees with those of *Kay et al.* [2008], who found that the increase in air temperatures and decrease in relative humidity during the summer of 2007 reduced cloudiness (i.e., *f*), increasing downwelling radiation (in shortwave by 32 W m^{-2}) and Arctic sea ice loss. However, the cloud effect was discussed in *Kay et al.* [2008] and *Kay and L'Ecuyer* [2013] only with respect to the aforementioned processes without considering any time lag. *Kapsch et al.* [2013] suggested that springtime transport of humid air increases cloudiness and downward longwave radiation, thus promoting sea ice melt after mid-May and decreasing downward shortwave radiation. The portion of longwave radiation that affects SIC was not investigated in this study. However, given our finding of strong ASR-SIC lagged correlation, the contribution of longwave radiation at least in June to summer sea ice melt may be small. In contrast, the decrease in clear-sky albedo due to sea ice melt increases net shortwave radiation, which compensates for cloudiness. Consistent with generally low correlations between *f* and ASR in Table 1, *Kapsch et al.* [2013] also suggested that the role of cloudiness in controlling sea ice is limited owing to the process such that the increase in net shortwave radiation amplifies any sea ice loss that has progressed with downward longwave radiation [*Francis et al.*, 2005; *Wu and Lee*, 2012].

We examined the spatial distribution of Arctic SIC responses to ASR to identify regions where SIC is more sensitive to ASR. Figure 6 shows the maximal covariance between −ASR and SIC (6a), the corresponding δSIC/δASR (6b), and the coefficient of determination (r^2) of SIC on −ASR in the case of the maximal covariance between −ASR and SIC (6c). The upper, and middle, and bottom panels represent late summer months (August, September, and October), respectively. It is apparent that the maximal covariance, the minimal δSIC/δASR, and r^2 have similar spatial patterns. The maximal value of covariance is 994.0 W m^{-2} %, and the minimal value of δSIC/δASR is −6.2% (W m^{-2})$^{-1}$. Based on the r^2 value in the grid-based ASR-SIC regression (Figure 6), ASR in the early summer months accounts for 40 to 80% of the total variance of Arctic SIC in the late summer months. Such sea ice areas comprise more than approximately 24% of the first-year/multi-year sea ice area (Table 2).

The significant values of covariance and δSIC/δASR are distributed annually between 80°N and 85°N. This latitudinal band corresponds to a transitional zone from multi-year ice to first-year ice. These significant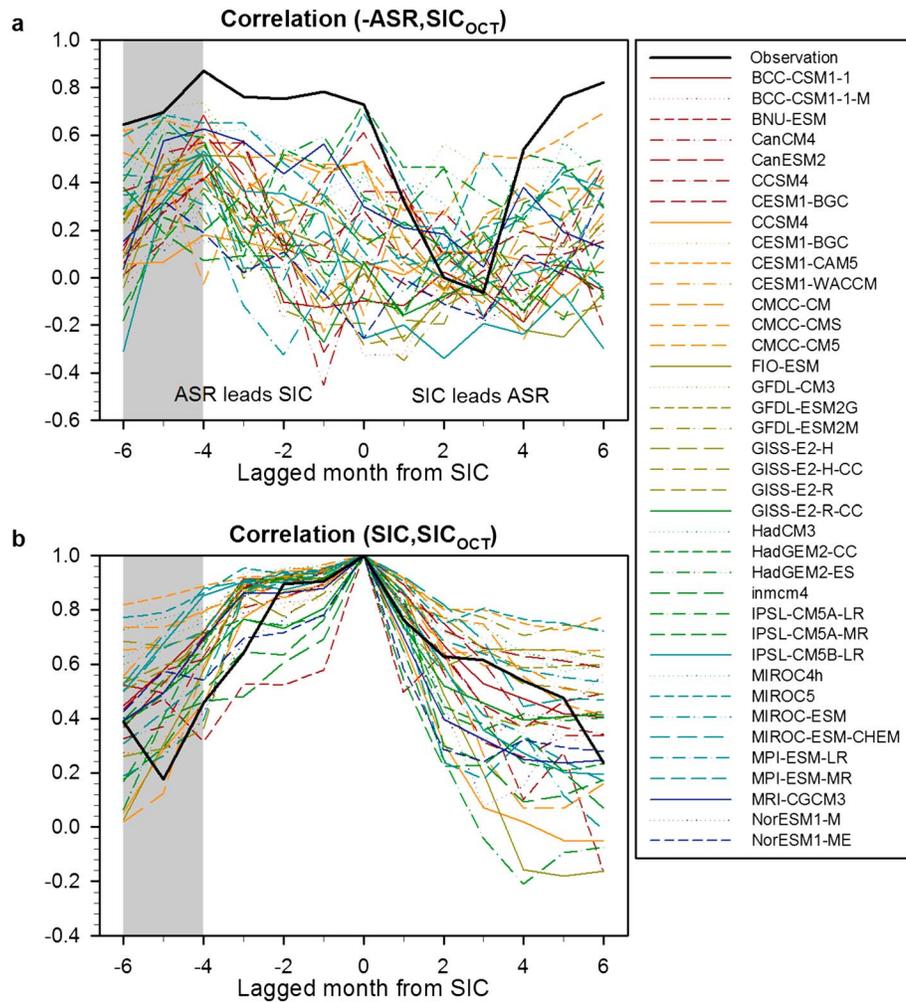 values are mostly concentrated on the north of the Chukchi Sea (denoted as C in Figure 6a). On the other hand, neither covariance nor δSIC/δASR exists over latitudes higher than 80°N in the presence of perennial sea ice, or near northern coasts of continents in the absence of summer sea ice. This is also true for the Kara and Barents Seas (denoted as K and B in Figure 6a), where first-year ice is dominant and sea ice does not exist in summer. There is also some influence associated with month. The area averages of maximum covariance over the Arctic Ocean are 184.9, 199.3, and 227.1 W m^{-2} % for the SICs in August, September, and October, respectively. Thus the area averages of covariance are higher in the later months (October > September > August) than in earlier months. In addition, the area averages of δSIC/δASR are −0.77, −0.96, and −0.84% (W m^{-2})$^{-1}$ for the SICs in August, September, and October, respectively.

The time lag for maximal covariance of −ASR and SIC is displayed in Figure 7. The time lags ranges from 0 to −4 months depending on regions. Dominant lags are −2, −3, and −4 months for August, September, and October, respectively, and are widely distributed over the East Siberian Sea. This figure reassures that SICs over the East Siberian Sea respond mainly to ASR in June. SICs at lower latitudes respond to ASR in July or August, resulting in a tendency for shorter time lags to occur in lower latitudes.

Figure 8. Lagged correlation coefficients between (a) −ASR and SIC in October and (b) SIC from observation data (thick black lines) and SIC from Coupled Model Intercomparison Project Phase 5 models (thin colored lines) in October.

3.2. Comparison With CMIP5 Models

The observed lagged correlation between ASR and SIC was compared against the corresponding lagged correlation modeled by historical runs of CMIP5 climate models (Figure 8). Note that the correlation coefficient is the covariance normalized by the variances of the two variables; thus, it accounts for the variation of ASR and SIC independently of the month. The lagged correlation between −ASR for all months against SIC in October and the lagged correlation between SIC for all months against SIC in October are shown in Figures 8a and 8b, respectively.

The inter-model differences in the lagged correlation between −ASR and SIC are notably large, and the models show maximum correlations in different months (Figure 8). This can be due to different magnitudes and phases of variation of cloud and ASR, as well as different ASR-SIC relationships that are implemented in models. In the observation, however, very strong correlation ($r \approx 0.88$) appears for a −4 months lag (note that the negative lag occurs when ASR leads SIC). This correlation is higher than those from any models and remains steady for the lagged month from −6 to 0 months. This pattern of correlation is different from covariance which has a maximum only at −4 months lag as shown Figure 5. SIC in October may eventually affect ASR in the following spring months (March to April, $r > 0.7$).

Sea ice is also influenced by thermal memory, and the autocorrelation of SIC persists for several months. However, at −4 months lag or less (as indicated by the shaded area in Figure 8b), the autocorrelation of SIC was observed to be very low, although it is relatively high in the climate models. The results shown in

Figure 8 therefore indicate that current climate models may underestimate the lagged solar radiation-sea ice connection, but over-emphasize internal sea ice processes when simulating SIC in late summer.

4. Summary and Discussion

The downward solar radiation at the surface has been regarded as an important factor in the thermodynamics of Arctic sea ice and the ice-albedo feedback in several studies [*Kapsch et al.*, 2013; *Perovich et al.*, 2008]. However, the solar radiation shielding effect of cloud on the ice-albedo feedback has not been investigated sufficiently. The findings of this study are distinguishable from previous studies in that the ASR-SIC relationship is carefully drawn with due consideration of cloud variations. The cloud shielding effect was investigated with flux and cloud parameters directly measured from the satellite, CERES.

The lagged correlation between ASR and SIC (ASR leads by 4 months) obtained from the satellite measurements was much greater than simulated in the CMIP5 climate models. Since the ASR anomaly in the spring/early summer (May–July) is largely controlled by cloud (and less so by ice/ocean surface conditions), this research suggests that current climate models cannot accurately simulate sea ice during the melt season without consideration of cloud radiative effects in spring/early summer.

Possible reasons for the time lags between ASR and SIC anomalies are discussed below. *Zhang* [2010] has also identified a similar lag correlation between the early summer surface air temperature (SAT) and the late summer sea ice extent from observations. As SAT is an indicator of surface energy budgets, the previous result supports our conclusion that TOA ASR plays a leading role in the decrease in SIC. At the top surface of the ice during summer, the downward solar energy is usually immediately absorbed and partly reflected. Observations at SHEBA (Surface Heat Budget of the Arctic Ocean) 1998 show that the cumulative total solar heat input to ice increases from March, but from June begins to greatly depend on ice albedo [*Perovich and Polashenski,* 2012]. Therefore, the solar input caused by any factor should be amplified by the ice-albedo feedback. Based on these observational findings, it is plausible that the solar heat input to the ice/ocean system in June determines the inter-annual variability of the total solar heat for the whole year. For example, the cumulative solar heat input to the ocean observed from the Beaufort Sea in 2007 increased gradually from June [*Perovich et al.*, 2008]. Our findings suggest that atmospheric cloud can be a major factor in altering this solar heat input in June, since the cloud shielding effect is most effective under the maximum TOA shortwave radiation. This cloud effect was, however, undetected by *Francis et al.* [2005], who emphasized the important role of longwave radiation in ice melting. This could potentially be attributed to the absence of recent data after 2005, as noted by *Kay et al.* [2008]. As the present study deals only with shortwave radiation, the potential leading role of longwave radiation in sea ice melting should be addressed in future work.

Given the importance of the ASR in June, another obvious extension of this work is to examine atmospheric circulation patterns and the resultant cloud distribution and solar input in June. A particular atmospheric circulation pattern such as anomalous high pressure over Beaufort Sea was found to enhance atmospheric and oceanic heat transport into the Pacific Arctic, which can cause the spring sea ice surface retreat and reduce surface albedo [*Zhang et al.*, 2008]. However, it is still in the vague whether this circulation change can be attributed to the rise in greenhouse gas emission forcing or unexpected natural climate variability. Further extensive studies are needed in this direction.

Large areas of the Arctic Ocean are now changing from sea ice to open sea. The enhanced heat and moisture fluxes from these newly generated open sea areas play an important role in the unprecedented Arctic warming observed in recent decades, particularly during the cold season [*Screen and Simmonds*, 2012; *Stroeve et al.*, 2014]. Therefore, a detailed investigation of the factors preceding decreases in Arctic sea ice is important for further understanding of the processes of Arctic warming. Moreover, it should be recognized that the impact of a warmer Arctic is not purely confined to this Arctic region: warming significantly weakens the surrounding polar jet, leading to favorable conditions for extreme weather patterns in some mid-latitude regions [*Francis and Vavrus*, 2012]. Therefore, the inconsistencies between the models and the observations noted above are critical for climate simulations, given the importance of sea ice for both local and remote impacts via significant Arctic warming.

References

Ackerman, S. A., R. E. Holz, R. Frey, E. W. Eloranta, B. C. Maddux, and M. McGill (2008), Cloud detection with MODIS. Part II: Validation, *J. Atmos. Oceanic Tech.*, *25*, 1073–1086.

CERES Science Team (2013), CERES ES4 Terra Edition3 Data Quality Summary. [Available at https://eosweb.larc.nasa.gov/sites/default/files/project/ceres/quality_summaries/CER_ES4_Terra_Edition3.pdf.]

Chang, L., J. Halvorson, E. Kizer, J. Robbins, J. Kibler, and D. Young (2013), Cloud and the Earth's Radiant Energy System (CERES) Data Management System: ES-4 Collection Guide, *NASA/LaRC ASDC*.

Coakley, J. A., Jr., M. A. Friedman, and W. R. Tahnk (2005), Retrieval of cloud properties for partly cloudy imager pixels, *J. Atmos. Oceanic Tech.*, *22*, 3–17.

Comiso, J. C., C. L. Parkinson, R. Gersten, and L. Stock (2008), Accelerated decline in the Arctic sea ice cover, *Geophys. Res. Lett.*, *35*, L01703, doi:10.1029/2007GL031972.

Day, J. J., J. C. Hargreaves, J. D. Annan, and A. Abe-Ouchi (2012), Sources of multi-decadal variability in Arctic sea ice extent, *Environ. Res. Lett.*, *7*, 034011.

Francis, J. A., and S. J. Vavrus (2012), Evidence linking Arctic amplification to extreme weather in mid-latitudes, *Geophys. Res. Lett.*, *39*, L06801, doi:10.1029/2012GL051000.

Francis, J. A., E. Hunter, J. R. Key, and X. Wang (2005), Clues to variability in Arctic minimum sea ice extent, *Geophys. Res. Lett.*, *32*, L21501, doi:10.1029/2005GL024376.

Hartmann, D. L. (1994), *Global Physical Climatology*, 411 pp., Academic Press, San Diego, Calif.

Kapsch, M.-L., R. G. Graversen, and M. Tjernström (2013), Springtime atmospheric energy transport and the control of Arctic summer sea-ice extent, *Nat. Clim. Change*, *3*, 744–748.

Kato, S., N. G. Loeb, D. A. Rutan, F. G. Rose, S. Sun-Mack, W. F. Miller, and Y. Chen (2012), Uncertainty estimate of surface irradiances computed with MODIS-, CALIPSO-, and CloudSat-derived cloud and aerosol properties, *Surv. Geophys.*, *26*, 2719–2740.

Kay, J. E., and A. Gettelman (2009), Cloud influence on and response to seasonal Arctic sea ice loss, *J. Geophys. Res.*, *114*, D18204, doi:10.1029/2009JD011773.

Kay, J. E., and T. L'Ecuyer (2013), Observational constraints on Arctic Ocean clouds and radiative fluxes during the early 21st century, *J. Geophys. Res. Atmos.*, *118*, 7219–7236, doi:10.1002/jgrd.50489.

Kay, J. E., T. L'Ecuyer, A. Gettelman, G. Stephens, and C. O'Dell (2008), The contribution of cloud and radiation anomalies to the 2007 Arctic sea ice extent minimum, *Geophys. Res. Lett.*, *35*, L08503, doi:10.1029/2008GL033451.

Kay, J. E., M. M. Holland, and A. Jahn (2011), Inter-annual to multi-decadal Arctic sea ice extent trends in a warming world, *Geophys. Res. Lett.*, *38*, L15708, doi:10.1029/2011GL048008.

Kinnard, C., C. M. Zdanowicz, D. A. Fisher, E. Isaksson, A. de Vernal, and L. G. Thompson (2011), Reconstructed changes in Arctic sea ice over the past 1,450 years, *Nature*, *479*, 509–512.

Kwok, R. (2009), Outflow of Arctic Ocean sea ice into the Greenland and Barents Seas: 1979–2007, *J. Clim.*, *22*, 2438–2457.

Kwok, R., G. F. Cunningham, and S. S. Pang (2004), Fram Strait sea ice outflow, *J. Geophys. Res.*, *109*, C01009, doi:10.1029/2003JC001785.

Lindsay, R., and J. Zhang (2005), The thinning of Arctic sea ice, 1988–2003: Have we passed a tipping point?, *J. Clim.*, *18*, 4879–4894.

Min, S.-K., X. Zhang, F. W. Zwiers, and T. Agnew (2008), Human influence on Arctic sea ice detectable from early 1990s onwards, *Geophys. Res. Lett.*, *35*, L21701, doi:10.1029/2008GL035725.

Overland, J. E., and M. Wang (2010), Large-scale atmospheric circulation changes are associated with the recent loss of Arctic sea ice, *Tellus A*, *62*, 1–9, doi:10.1111/j.1600-0870.2009.00421.x.

Parkinson, C. L., and J. C. Comiso (2013), On the 2012 record low Arctic sea ice cover: Combined impact of preconditioning and an August storm, *Geophys. Res. Lett.*, *40*, 1356–1361, doi:10.1002/grl.50349.

Perovich, D. K., and C. Polashenski (2012), Albedo evolution of seasonal Arctic sea ice, *Geophys. Res. Lett.*, *39*, L08501, doi:10.1029/2012GL051432.

Perovich, D. K., J. A. Richter-Menge, K. F. Jones, and B. Light (2008), Sunlight, water, and ice: Extreme Arctic sea ice melt during the summer of 2007, *Geophys. Res. Lett.*, *35*, L11501, doi:10.1029/2008GL034007.

Perovich, D. K., K. F. Jones, B. Light, H. Eicken, T. Markus, J. Stroeve, and R. Lindsay (2011), Solar partitioning in a changing Arctic sea-ice cover, *Ann. Glaciol.*, *52*, 192–196.

Polyakov, I. V., et al. (2010), Arctic Ocean warming contributes to reduced polar ice cap, *J. Phys. Oceanogr.*, *40*, 2743–2756.

Ramanathan, V. (1987), The role of earth radiation budget studies in climate and general circulation research, *J. Geophys. Res.*, *92*, 4075–4095, doi:10.1029/JD092iD04p04075.

Rayner, N. A., D. E. Parker, E. B. Horton, C. K. Folland, L. V. Alexander, D. P. Rowell, E. C. Kent, and A. Kaplan (2003), Global analyses of sea surface temperature, sea ice, and night marine air temperature since the late nineteenth century, *J. Geophys. Res.*, *108*(D14), 4407, doi:10.1029/2002JD002670.

Rigor, I. G., J. M. Wallace, and R. L. Colony (2002), Response of sea ice to the Arctic Oscillation, *J. Clim.*, *15*, 2648–2668.

Riihelä, A., T. Manninen, and V. Laine (2013), Observed changes in the albedo of the Arctic sea-ice zone for the period 1982–2009, *Nat. Clim. Change*, *3*, 895–898.

Schweiger, A. J., R. W. Lindsay, S. Vavrus, and J. A. Francis (2008), Relationships between Arctic sea ice and clouds during autumn, *J. Clim.*, *21*, 4799–4810.

Screen, J. A., and I. Simmonds (2012), Declining summer snowfall in the Arctic: Causes, impacts and feedbacks, *Clim. Dyn.*, *38*, 2243–2256.

Stroeve, J. C., M. Serreze, S. Drobot, S. Gearheard, M. Holland, J. Maslanik, W. Meier, and T. Scambos (2008), Arctic sea ice extent plummets in 2007, *Eos. Trans. AGU*, *89*, 13–14, doi:10.1029/2008EO020001.

Stroeve, J. C., V. Kattsov, A. Barrett, M. Serreze, T. Pavlova, M. Holland, and W. N. Meier (2012a), Trends in Arctic sea ice extent from CMIP5, CMIP3 and observations, *Geophys. Res. Lett.*, *39*, L16502, doi:10.1029/2012GL052676.

Stroeve, J. C., M. C. Serreze, J. E. Kay, M. M. Holland, W. N. Meier, and A. P. Barrett (2012b), The Arctic's rapidly shrinking sea ice cover: A research synthesis, *Clim. Change*, *110*, 1005–1027.

Stroeve, J. C., T. Markus, L. Boisvert, J. Miller, and A. Barrett (2014), Changes in Arctic melt season and implications for sea ice loss, *Geophys. Res. Lett.*, *41*, doi:10.1002/2013GL058951.

Taylor, K. E., R. J. Stouffer, and G. A. Meehl (2011), An Overview of CMIP5 and the experiment design, *Bull. Am. Meteorol. Soc.*, *93*, 485–498.

Wielicki, B. A., B. R. Barkstrom, E. F. Harrison, R. B. Lee III, G. Louis Smith, and J. E. Cooper (1996), Clouds and the Earth's Radiant Energy System (CERES): An earth observing system experiment, *Bull. Am. Meteorol. Soc.*, *77*, 853–868.

Wu, D. L., and J. N. Lee (2012), Arctic low cloud changes as observed by MISR and CALIOP: Implication for the enhanced autumnal warming and sea ice loss, *J. Geophys. Res.*, *117*, D07107, doi:10.1029/2011JD017050.

Zhang, J., R. Lindsay, A. Schweiger, and M. Steele (2013), The impact of an intense summer cyclone on 2012 Arctic sea ice retreat, *Geophys. Res. Lett.*, *40*, 720–726, doi:10.1002/grl.50190.

Zhang, X. (2010), Sensitivity of arctic summer sea ice coverage to global warming forcing: Towards reducing uncertainty in arctic climate change projections, *Tellus A*, *62A*, 220–227.

Zhang, X., M. Ikeda, and J. E. Walsh (2003), Arctic sea ice and freshwater changes driven by the atmospheric leading mode in a coupled sea ice-ocean model, *J. Clim.*, *16*, 2159–2177.

Zhang X., A. Sorteberg, J. Zhang, R. Gerdes, and J. C. Comiso (2008), Recent radical shifts of atmospheric circulations and rapid changes in Arctic climate system, *Geophys. Res. Lett.*, *35*, L22701, doi:10.1029/2008GL035607.